Local modes and localization in a multicomponent nonlinear lattice

Kyle Forinash,[1] Thierry Cretegny,[2,3] and Michel Peyrard[2,4]

[1]*Indiana University Southeast, New Albany, Indiana 47150*

[2]*Laboratoire de Physique de l'Ecole Normale Supérieure de Lyon, CNRS URA 1325, 46 allée d'Italie, 69007 Lyon, France*

[3]*Laboratoire Léon Brillouin, CE Saclay, 91 191 Gif-sur-Yvette, France*

[4]*CNLS, MS B258, Los Alamos National Laboratory, Los Alamos, New Mexico 87545*

(Received 25 October 1996)

The existence, stability, and the conditions for the formation of nonlinear localized modes are investigated in a two-component one-dimensional lattice. In spite of their possible coupling with acoustic phonons, discrete breathers can exist as exact stable solutions or show a very slow decay. Nonlinear energy localization through energy exchange between localized excitations, exhibited previously for a one-component lattice [T. Dauxois and M. Peyrard, Phys. Rev. Lett. **70**, 3935 (1993)] is more general and also valid in a multicomponent lattice. A self-localization of thermal fluctuations is also observed in such a system. The model is used to investigate the effect of bending proteins on DNA. It shows that a bend can collect the energy of moving localized modes or insulate one part of the molecule from transfers of energy from large amplitude excitations in other parts. [S1063-651X(97)05504-9]

I. INTRODUCTION

Numerous studies have been devoted to localized modes in nonlinear lattices because they provide examples of localized excitations in *homogeneous* lattices, i.e., in the absence of any disorder. Approximate solutions have been obtained for one-dimensional or multidimensional lattices [1] and a proof of existence of time-periodic, spatially localized, solutions, or breathers, has been given for a broad range of Hamiltonian coupled oscillators lattices [2,3]. Moreover, a *spontaneous* localization of energy in such lattices has been found and it has been shown that it can occur through energy exchange between interacting moving breathers [4].

However, these studies have considered lattices with *one degree of freedom per site* while most of the physical systems are multicomponent systems. Extending the results to a multicomponent lattice is not necessarily trivial because interactions among the various degrees of freedom could destroy the local modes since they provide additional pathways for energy flow in the lattice. Our aim here is to consider a simple example of a multicomponent system and investigate to what extent the properties of simpler nonlinear lattices remain valid. The model that we have considered is a two-chain model for describing the dynamics of DNA and its thermal denaturation [5]. It has been chosen because it provides a simple two-component model to examine the questions listed above, and because it may be relevant to study some important biological properties of DNA, such as the relation between bending and local opening, which may be significant for the initiation of the transcription since the RNA polymerase bends DNA locally while it creates the transcription bubble [6,7], or the possible exchange of energy between acoustic and optical modes in the molecule which could be stimulated, for instance, by ultrasonic excitations.

The questions that we have particularly examined are the following: (i) the existence and stability of local modes in a two-chain nonlinear lattice (Sec. III), (ii) the interactions between local modes as a mechanism for energy localization (Sec. IV), and (iii) the role of bending on DNA local opening (Sec. V).

II. MODEL

The Hamiltonian of the system is

$$H' = \sum_n \frac{1}{2} m \left[\left(\frac{du_n}{dt'} \right)^2 + \left(\frac{dv_n}{dt'} \right)^2 \right] + \frac{1}{2} k (u_{n+1} - u_n)^2$$
$$+ \frac{1}{2} k' (v_{n+1} - v_n)^2 + D \{ \exp[-a(u_n - v_n)] - 1 \}^2.$$

(1)

The two degrees of freedom per cell, u_n and v_n, describe the transverse displacements of the two bases belonging to the base pair labeled by index n in the DNA molecule [5]. The coupling of two nucleotides along the same strand is assumed to be harmonic, with coupling constants k and k'. Paired bases in DNA are always different from each other. In a homopolymer formed, for instance, only of adenine-thymine (A-T) pairs, the interactions along the two strands involve the stacking of bases with a single cycle on one strand, while on the other strand two-cycle bases are stacked. In natural DNA with a complicated base sequence, the differences between the two strands tend to be averaged out, but, on a segment of the molecule with a size of the order of the size of a transcription bubble, i.e., 20 base pairs, the difference between the strands is still very large. To appreciate this, one may notice that the stacking energies of the different base pairs in DNA vary at a ratio of 1 to 6, depending on the stacked bases [8]. Moreover, if the molecule is bent, this brings the bases inside the bend closer to each other, and increases their interaction significantly, which is another cause for the absence of symmetry between the two strands. Therefore, k and k' can be very different. As we shall see below, this has important consequences. The interaction between the two bases in a pair is modeled by a Morse

potential, which represents the hydrogen bonds coupling the bases, as well as the repulsive interaction between the phosphate groups.

Introducing dimensionless displacements $U_n = au_n$ and $V_n = av_n$, and a dimensionless time $t = t'\sqrt{m/Da^2}$, we get a dimensionless Hamiltonian $H = H'/D$ under the form

$$H = \sum_n \frac{1}{2}\left[\left(\frac{dU_n}{dt}\right)^2 + \left(\frac{dV_n}{dt}\right)^2\right] + \frac{1}{2}K(U_{n+1} - U_n)^2$$

$$+ \frac{1}{2}K'(V_{n+1} - V_n)^2 + \{\exp[-(U_n - V_n)] - 1\}^2, \quad (2)$$

where the dimensionless coupling constants are $K = k/Da^2$, $K' = k'/Da^2$.

The equations of motion deriving from Hamiltonian (2) are

$$\frac{d^2U_n}{dt^2} = K(U_{n+1} + U_{n-1} - 2U_n)$$

$$+ 2e^{-(U_n - V_n)}(e^{-(U_n - V_n)} - 1), \quad (3a)$$

$$\frac{d^2V_n}{dt^2} = K'(V_{n+1} + V_{n-1} - 2V_n)$$

$$- 2e^{-(U_n - V_n)}(e^{-(U_n - V_n)} - 1). \quad (3b)$$

It is interesting to consider the new variables

$$X_n = \frac{U_n + V_n}{\sqrt{2}}, \quad Y_n = \frac{U_n - V_n}{\sqrt{2}}, \quad (4)$$

where X_n describes the acoustic motions of the two-chain system, while Y_n corresponds to the stretching of the bond connecting the two strings. If we introduce the coupling constants

$$K_+ = \frac{K + K'}{2}, \quad K_- = \frac{K - K'}{2}, \quad (5)$$

the equations of motion become

$$\frac{d^2X_n}{dt^2} - K_+(X_{n+1} + X_{n-1} - 2X_n)$$

$$= K_-(Y_{n+1} + Y_{n-1} - 2Y_n), \quad (6a)$$

$$\frac{d^2Y_n}{dt^2} - K_+(Y_{n+1} + Y_{n-1} - 2Y_n) - \frac{4}{\sqrt{2}}e^{-\sqrt{2}Y_n}(e^{-\sqrt{2}Y_n} - 1)$$

$$= K_-(X_{n+1} + X_{n-1} - 2X_n). \quad (6b)$$

Equations (6) show that, for the symmetric case $K = K'$, i.e., $K_- = 0$, the X and Y motions are decoupled. The acoustic motions are then simply linear and nonlinearity shows up only in the stretching mode Y. In this case, a separate study of the stretching motion is possible. We are interested here in the more general case $K \neq K'$, so that the X and Y motions are not independent of each other.

The dispersion relations of the small amplitude waves of frequency ω and wave vector q are given by
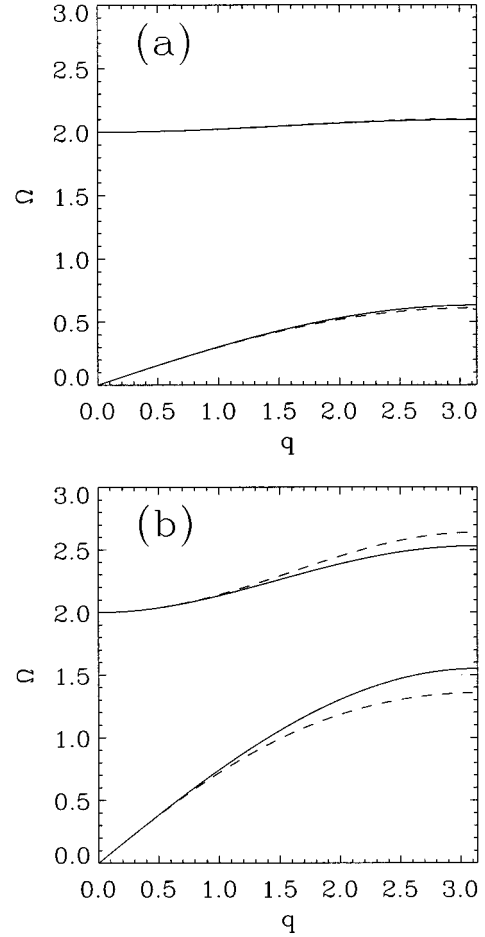

FIG. 1. Dispersion curves of the two-chain model. (a) $K_+ = 0.1$, $K_- = 0$ (full lines) and $K_- = 0.08$ (dashed lines), (b) $K_+ = 0.6$, $K_- = 0$ (full lines) and $K_- = 0.4$ (dashed lines).

$$\omega^2 = 2\left(1 + 2K_+\sin^2\frac{q}{2}\right) \pm 2\sqrt{1 + 4K_-^2\sin^4(q/2)}, \quad (7)$$

where the $+$ sign corresponds to the optical branch (which involves only the stretching Y if $K_- = 0$) and the $-$ sign corresponds to the acoustic branch (which involves only X if $K_- = 0$). Figure 1 shows these dispersion relations in two typical cases, a weak coupling case $K_+ = 0.1$ and a stronger coupling $K_+ = 0.6$. The coupling between the two motions for $K_- \neq 0$ shows up in the modification of the dispersion relation. When K_- increases, the optical band reaches higher values for large q while the maximum acoustic frequency decreases, increasing the gap between the acoustic and optical bands which exists as long as the coupling is not too large. However, as shown in Fig. 1, the change is only significant at large coupling.

III. EXISTENCE AND STABILITY OF LOCAL MODES

A. Existence and exact solutions

For Hamiltonian lattices of coupled nonlinear oscillators with a one-component degree of freedom, a rigorous proof of the existence of nonlinear localized modes has been obtained [2,3]. Such modes exist, provided that the coupling is below a threshold which depends on their amplitude. This proof is

also valid for the two-chain model if $K_- = 0$, because then the Y degree of freedom, which carries the nonlinearity, is totally decoupled from X and can be studied separately. In this case Eq. (6b) reduces to

$$F_n(\mathbf{Y}, K_+) = \ddot{Y}_n + K_+(Y_{n+1} + Y_{n-1} - 2Y_n) + \mathcal{V}'(Y_n) = 0, \quad (8)$$

where $\mathcal{V}(Y) = D[\exp(-\sqrt{2}Y) - 1]^2$ is the on-site potential.

The idea of the proof is to consider the *anticontinuum* limit $K_+ \to 0$, where the coupling vanishes. In this limit, the existence of localized solutions is trivial because the oscillators are uncoupled. The localized modes that we are looking for here are *breathers*, i.e., oscillatory modes characterized by a given frequency Ω. Therefore, among all the possible solutions in the anticontinuum limit, only the solutions that satisfy the following conditions are considered: (i) for all n $Y_n(t)$ is periodic in time $Y_n(t) = Y_n(t + 2\pi/\Omega)$; (ii) the solution is time reversible $Y_n(t) = Y_n(-t)$. Such solutions can be characterized by a set of numbers defining a code $\{\sigma_n\}$, such that $\sigma_n = 0$ when an oscillator is at rest, $\sigma_n = m$ if the frequency of the nth oscillator is $m\Omega$ (m integer) and its phase at $t = 0$ is 0, and $\sigma_n = -m$ if the frequency is $m\Omega$ and the initial phase is π. In particular, the anticontinuum limit solution which corresponds to a breather centered on the site n_0 is simply defined by $\sigma_{n_0} = 1$ and $\sigma_n = 0$ if $n \neq n_0$.

It is remarkable that the trivial solution of $\mathbf{F}(\mathbf{Y}, 0) = \mathbf{0}$ for decoupled oscillators has a unique continuation $Y_n(t, K_+)$ for finite coupling K_+, as long as the coupling is below a given threshold $K_+ < K_c$; conditions for this continuation are (i) $\partial\omega(I)/\partial I \neq 0$ for the frequencies $i\Omega$ that appear in the code $\{\sigma_n\}$ of the configuration, where I is the action of a single oscillator represented in action-angle variables, (ii) $m\Omega \neq \sqrt{\mathcal{V}'(0)}$ for all m appearing in the code of the configuration. The first condition implies that the oscillators must be *nonlinear*, as their frequency depends on their action. This condition is easy to understand intuitively because we consider a lattice made of identical oscillators. If they were linear, any excitation of one of them would be in exact resonance with the neighbors and any weak coupling would allow the energy of an excited site to be transferred to its neighbors. The second condition, which could be relaxed if one looks at nonlocalized solutions, such that $\sigma_n \neq 0$ for all n, is also a nonresonance condition. The breather frequency Ω and its harmonics that enter in the solution must not resonate with the linear frequency of the oscillators. Among all the solutions defined by their code $\{\sigma_n\}$, the breather solution $\sigma_{n_0} = 1$ and $\sigma_n = 0$ if $n \neq n_0$ is characterized by an exponential decay of the amplitude as a function of $|n - n_0|$.

For $K_- \neq 0$, the X and Y degrees of freedom are coupled. However, *the proof of existence of localized oscillatory solutions can be extended* to this multicomponent system [10]. The method amounts to eliminating the acoustic variable, which is coupled to the optical one, through the dynamical equations of motions. For a one-dimensional lattice this is always possible and the theorem established for a one-component model can be extended to the two-chain model that we consider here, so that the existence of localized breather modes at low coupling can also be established.

Moreover, the introduction of the anticontinuum limit goes beyond a proof of existence because it can also provide

a numerical method to actually derive an exact solution [11]. Let us denote, by the generic notation q_i, the degrees of freedom corresponding to the positions X_i and Y_i and by p_i the conjugate variables. A breather of period T_b is a fixed point of the operator $\mathcal{T}$ which associates the configuration at time T_b to a given initial configuration $(\mathbf{q}, \mathbf{p}) = (\{q_i\}\{p_i\})$. Moreover, as the equations of motion are invariant under time reversal, we can restrict the search to initial configurations where all the sites are initially at rest ($p_i = 0 \ \forall i$), i.e., we start from a maximum of the breather amplitude. For N sites, $\mathcal{T}$ is therefore, an application from $\mathbb{R}^{2N}$ (for the two-component model) to $\mathbb{R}^{4N}$. Finding an exact solution of period T_b amounts, therefore, to finding a zero of the operator

$$O(\mathbf{q}) = \mathcal{T}(\mathbf{q}, \mathbf{0}) - (\mathbf{q}, \mathbf{0}). \quad (9)$$

The numerical method solves this equation by expanding $O(\mathbf{q})$ around an approximate solution $\mathbf{q}_0$ as

$$O(\mathbf{q}) = O(\mathbf{q}_0) + \mathcal{A} \times (\mathbf{q} - \mathbf{q}_0), \quad (10)$$

where $\mathcal{A}$ is a $4N \times 2N$ matrix, and minimizing the norm of $O(\mathbf{q})$ with respect to q. Using energy conservation one could restrict the calculation to the first $2N$ components q_i since, if the initial positions are exactly reproduced at time T_b, the momenta have to vanish to conserve energy. The anticontinuum limit provides the necessary approximate solution $\mathbf{q}_0$ because, in the limit of vanishing coupling, the breather reduces to the motion of a particle in the Morse potential which can be solved exactly. The numerical method starts from the exact solution with $K_+ = K_- = 0$ and increases the coupling in small steps. For each step, Eq. (9) is solved with a starting approximate solution $\mathbf{q}_0$ which is the exact solutions obtained at the previous step. Although the principle of the calculation is simple, there are several technical problems which are discussed in [11,16]. For instance, when the system has solutions at frequency 0 (such as the acoustic translational mode of the two-component chain) or multiple of the breather frequency $\omega_b = 2\pi/T_b$, the reduced $2N \times 2N$ matrix $\mathcal{A}$ is not invertible, although Eq. (9) has an exact solution.

When the exact solution has been found, its linear stability can be investigated by the Floquet method, i.e., by looking for the time evolution over one period of a small perturbation $(\delta\mathbf{q}(0), \delta\mathbf{p}(0))$. A linearization leads to the value of the perturbation at time T_b as

$$(\delta\mathbf{q}(T_b), \delta\mathbf{p}(T_b)) = \mathcal{F} \times (\delta\mathbf{q}(0), \delta\mathbf{p}(0)), \quad (11)$$

where $\mathcal{F}$ is the Floquet matrix. The solution is stable if the perturbation decays in time; i.e., the modulus of all the eigenvalues of $\mathcal{F}$ is lower or equal to 1 (the eigenvalue 1 is always present and simply corresponds to a time translation of the breather solution).

B. Approximate solution

Since we have an exact solution, one may wonder whether it is useful to look for an approximate solution. However, the exact solution can only be obtained numerically, and, moreover, only nonmoving modes can be obtained. The lattice breaks the continuous translation and ex-

act moving solutions do not exist. However, when the coupling is sufficient or when the amplitude of the local mode is small, approximate moving solutions can exist. Although we expect these solutions to be trapped by discreteness effects [9], they can be relevant in a physical system, in particular as transient states leading to energy localization (See Sec. IV). They can be obtained analytically in the continuum limit with a multiple scale expansion if the coupling constant K_- is sufficiently small. The nonlinear term of Eq. (6b) is expanded as

$$\frac{4}{\sqrt{2}}e^{-\sqrt{2}Y_n}(e^{-\sqrt{2}Y_n}-1)=4(Y_n+\alpha Y_n^2+\beta Y_n^3),$$

$$\text{with} \quad \alpha=-\tfrac{3}{2}\sqrt{2}, \quad \beta=\tfrac{7}{3}. \quad (12)$$

If we look for solutions of order ϵ, $X=\epsilon\psi$ and $Y=\epsilon\phi$, with $K_+=c_0^2$ being of order 1 while $K_-=\epsilon c'^2_0$ is assumed to be of order ϵ, Eqs. (6a) in the continuum limit become

$$\frac{\partial^2\psi}{\partial t^2}-c_0^2\frac{\partial^2\psi}{\partial x^2}=\epsilon c'^2_0\frac{\partial^2\phi}{\partial x^2}, \quad (13)$$

$$\frac{\partial^2\phi}{\partial t^2}-c_0^2\frac{\partial^2\phi}{\partial x^2}+\omega_0^2(\phi+\epsilon\alpha\phi^2+\epsilon^2\beta\phi^3)=\epsilon c'^2_0\frac{\partial^2\psi}{\partial x^2}, \quad (14)$$

where we have introduced the constant $\omega_0^2=4$ for convenient tracking of the various contributions in the following formulas. Looking for a solution of the form

$$\phi=\phi_0+\epsilon\phi_1+\epsilon^2\phi_2, \quad \psi=\psi_0+\epsilon\psi_1+\epsilon^2\psi_2, \quad (15)$$

where the functions ψ_i and ϕ_i depend on the multiple scale variables $T_0=t$, $T_1=\epsilon t$, $T_2=\epsilon^2 t$ and $X_0=x$, $X_1=\epsilon x$, $X_2=\epsilon^2 x$, at order ϵ^0 we get

$$\phi_0=A(X_1,T_1,X_2,T_2)e^{i(q_1X_0-\omega_1T_0)}+\text{c.c.}=Ae^{i\theta_1}+\text{c.c.}, \quad (16)$$

$$\psi_0=B(X_1,T_1,X_2,T_2)e^{i(q_2X_0-\omega_2T_0)}+\text{c.c.}=Be^{i\theta_2}+\text{c.c.}, \quad (17)$$

where the phase factors θ_1 and θ_2, which depend on the fast variables X_0,T_0, can be chosen independently, provided that ω_1 and ω_2 obey the continuous dispersion relations

$$\omega_1^2=\omega_0^2+c_0^2q_1^2 \quad \omega_2^2=c_0^2q_2^2. \quad (18)$$

This freedom in the selection of the phase factors comes from the assumption that K_- is of the order ϵ.

At order ϵ, the cancellations of the secular terms give the conditions

$$\frac{\partial A}{\partial T_1}=-V_{g1}\frac{\partial A}{\partial X1} \quad \text{with} \quad V_{g1}=\frac{q_1c_0^2}{\omega_1}, \quad (19a)$$

$$\frac{\partial B}{\partial T_1}=-V_{g2}\frac{\partial B}{\partial X1} \quad \text{with} \quad V_{g2}=\frac{q_2c_0^2}{\omega_2}, \quad (19b)$$

and the solution of the remaining equations gives the first order contributions

$$\phi_1=\alpha\left(-2|A|^2+\frac{1}{3}A^2e^{2i\theta_1}+\frac{1}{3}A^{*2}e^{-2i\theta_1}\right)$$
$$-\frac{q_2^2c'^2_0}{\omega_0^2}(Be^{i\theta_2}+B^*e^{-i\theta_2}), \quad (20a)$$

$$\psi_1=\frac{q_1^2c'^2_0}{\omega_0^2}(Ae^{i\theta_1}+A^*e^{-i\theta_1}). \quad (20b)$$

Finally, at order ϵ^2, the cancellations of the secular terms give equations for A and B.

For A we obtain

$$i\frac{\partial A}{\partial\tau_2}+P\frac{\partial^2 A}{\partial\xi_1^2}+Q|A|^2A-RA=0, \quad (21)$$

with

$$P=\frac{c_0^2\omega_0^2}{2\omega_1^3}, \quad Q=\frac{\omega_0^2}{2\omega_1}\left(\frac{10}{3}\alpha^2-3\beta\right), \quad R=\frac{q_1^4c'^4_0}{2\omega_1\omega_0^2}. \quad (22)$$

Equation (21) is written in the frame moving at speed V_{g1}, i.e., $\xi_1=X_1-V_{g1}T_1$, $\tau_2=T_2$. It can be brought to the standard nonlinear Schrödinger (NLS) form by defining $A=A'\exp(-iR\tau_2)$ to get

$$i\frac{\partial A'}{\partial\tau_2}+P\frac{\partial^2 A'}{\partial\xi_1^2}+Q|A'|^2A'=0. \quad (23)$$

For the parameters ω_0, α, β considered here, the product PQ is positive and the equation has the standard soliton solution of amplitude A_0 and envelope velocity v_e

$$A'=A_0\text{sech}[\sqrt{(Q/2P)}A_0(\xi_1-v_e\tau_2)]\exp\left(i\frac{v_e\xi_1}{2P}\right)$$
$$\times\exp\left[-i\left(\frac{v_e^2}{4P}-\frac{QA_0^2}{2}\right)\tau_2\right]. \quad (24)$$

For B we obtain the *linear* equation

$$i\frac{\partial B}{\partial T_2}+\frac{q_2^4c'^4_0}{2\omega_2\omega_0}B=0. \quad (25)$$

This equation has plane wave solutions. Therefore, if we look for localized modes, we must chose $B=0$.

Using Eqs. (15), (20a), and (24), one can get the expression for the X and Y solutions up to order ϵ. The expansion parameter ϵ can be eliminated if we express the solution as a function of the amplitude $a_0=\epsilon A_0$, envelope velocity $V_e=\epsilon v_e$, and wave vector q_1, and we get

$$Y(x,t)=2a_0\text{sech}\{\omega_1\sqrt{(\delta/2K_p)}a_0[x-(V_{g1}+V_e)t]\}$$
$$\times\cos(\kappa x-\Omega t)+\sqrt{2}\,a_0^2\text{sech}^2\{\omega_1\sqrt{(\delta/2K_p)}$$
$$\times a_0[x-(V_{g1}+V_e)t]\}[3-\cos(2\kappa x-2\Omega t)],$$

$$(26a)$$

$$X(x,t)=2\frac{q_1^2 K_-}{\omega_0^2}a_0\mathrm{sech}\{\omega_1\sqrt{(\delta/2K_p)}$$

$$\times a_0[x-(V_{g1}+V_e)t]\}\cos(\kappa x-\Omega t),\quad (26b)$$

where

$$\omega_1^2=\omega_0^2+K_+q_1^2,\quad \omega_0^2=4,\qquad (27a)$$

$$\kappa=q_1+\frac{V_e\omega_1^3}{K_+\omega_0^2},\quad V_{g1}=\frac{q_1 K_+}{\omega_1},\qquad (27b)$$

$$\Omega=\omega_1-a_0^2\delta\frac{\omega_0^2}{4\omega_1}+\frac{(V_e+2V_{g1})V_e\omega_1^3}{2\omega_0^2 K_+}+\frac{q_1^4 K_-^2}{2\omega_1\omega_0^2},$$

$$\delta=\frac{10}{3}\alpha^2-3\beta=8.\qquad (27c)$$

C. Numerical tests of existence and stability

The exact solutions derived above for a finite chain with periodic boundary conditions can be tested for stability in an infinite lattice by numerically solving the equations of motion (3). An initial condition is calculated for a lattice with N_0 cells, chosen large enough to include all the domains where the breather oscillations have a significant amplitude (more than $\approx 10^{-7}$ the maximum amplitude). Depending on the coupling constant this may require $20 \leq N_0 \leq 40$. Then this solution is embedded in a much larger lattice including N cells ($N=100$ or 200) with two end regions of 10 cells, where we introduce damping that grows linearly toward the ends. These damped regions can absorb all the small amplitudes waves that could be emitted by an unstable breather. Simulations have been performed with a fifth order Runge-Kutta scheme or a fourth order symplectic integrator which guarantees a perfect energy conservation [12,13]. With a time step $\Delta t=0.01$, in the absence of damping, the energy is conserved to a relative accuracy of 10^{-7} over a whole simulation. This does not depend on the total time interval investigated (typically 20 000 to 80 000 time units) because the symplectic integrator prevents any drift of the mean value of the energy, although the energy may fluctuate around its mean value when the time step is large. Using such an integrator allows us to check the stability of a breather by calculating the energy E_0 within the domain size N_0 that contained the initial breather. When the breather is perfectly stable, the simulation checks that E_0 stays exactly constant (to an accuracy of 10^{-7}). If there is an instability, even very weak, energy flows away from the domain of size N_0. Thus E_0 differs from the total energy E and, when the emitted waves reach the damped domains near the boundaries, E starts to decrease.

1. K=K', one-component system

In order to understand the possible sources of instability of a breather, it is useful to start from the simplest case of a symmetric model $K=K'$, which is equivalent to a one-component model for the optical motion Y. The proof of existence indicates that breathers exist only below a critical coupling K_c, but it does not provide an explicit value of
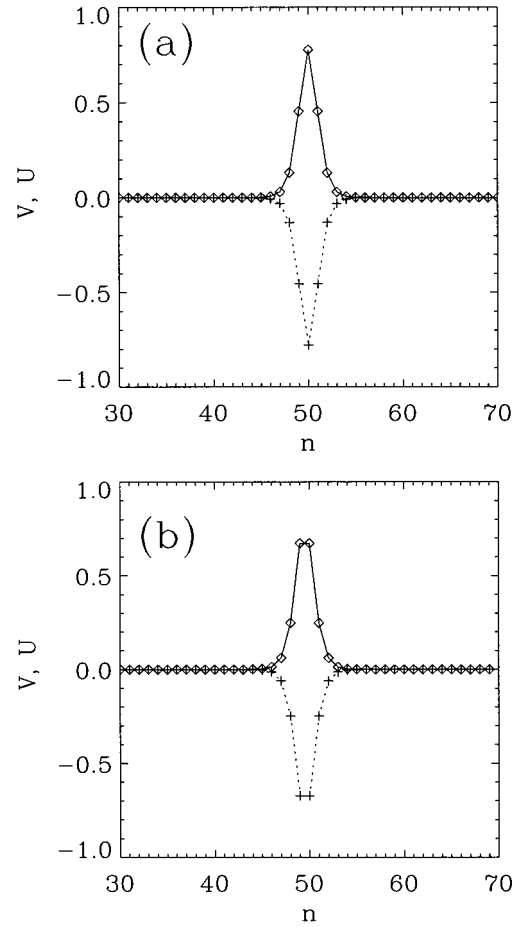

FIG. 2. Exact breather solution for $K=K'=0.6$, $\Omega=1.6$. (a) One-breather solution (centered breather). This solution is unstable. (b) Stable two-breather solution (noncentered breather). The diamonds and crosses show the initial positions of U_n and V_n, respectively.

K_c. Numerical tests show that, as far as the *existence* of an solution is concerned, the maximum allowed coupling is high. Figure 2(a) shows an example with $K=K'=0.6$ for a breather frequency $\Omega=1.6$. The Floquet analysis finds, however, one eigenvalue equal to 1.3 for this solution, indicating a rather strong instability. The corresponding eigenvector or the numerical simulation can explain the reason for this instability: in the simulation, after a very short transient the breather radiates a small amount of energy and its center moves by half a lattice spacing. We recover here a result previously found for a discrete ϕ^4 model [14,15]: in a discrete lattice a breather centered on a lattice site does not always correspond to the stable solution. The stable solution for the same coupling constants and frequency is shown in Fig. 2(b). It can be viewed as a breather centered *between* two lattice sites and will, henceforth, be called a noncentered breather. In the language of the anticontinuum limit this solution should rather be called a ''multibreather,'' since it is generated by the initial excitation of two sites (its code $\{\sigma_n\}$ is given by $\sigma_{n_0}=1$, $\sigma_{n_0-1}=1$, all other $\sigma_n=0$). For the whole zone of the parameter space (K_+,Ω) which was explored, the centered and noncentered breathers have the same domain of existence, and generally only one of the two is stable (the one with maximum action $\int_0^T L\,dt$, where T is
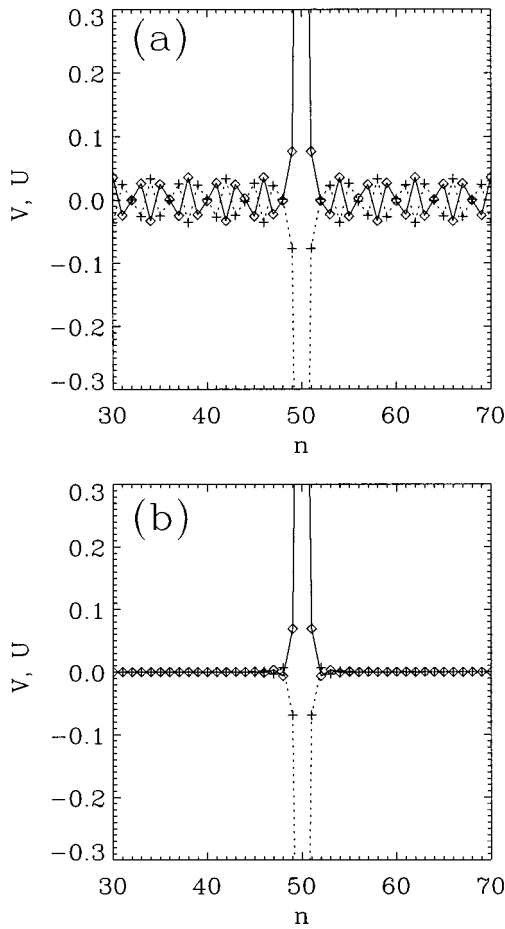
FIG. 3. Breather shape for $K = K' = 0.1$ and $\Omega = 1.04$ (a) such that $2\ \Omega$ is within the optical band or $\Omega = 1.06$ (b) for which $2\ \Omega$ is above the optical band. The diamonds and crosses show the initial positions of U_n and V_n, respectively.

the period of the breather and L the Lagrangien of the system) while the other is unstable [16]. Thus some instabilities, such as in the preceding example, are not of physical relevance; they merely imply that, at this frequency, the stable solution is not the one-breather solution but the noncentered ''bibreather.''

This simple example illustrates one channel by which a single breather can become unstable. However, in such a case, this does not mean that a localized solution with the same frequency does not exist, but merely that the stable solution is not the ''one-breather'' solution. There are more fundamental sources of instability. Figure 3(a) shows the exact solution obtained for $K = K' = 0.1$, $\Omega = 1.04$. In this case the amplitude of the oscillations does not decay when one moves away from the breather center. The breather appears to be superimposed on a plane wave of optical character as the U and V displacements are in opposition of phase. In the Floquet analysis made on a lattice with $N_0 = 40$ cells with periodic boundary conditions, this solution is found to be *linearly stable*. However, this is not the case when it is used as an initial condition for a simulation in a longer chain with absorbing ends. Energy flows away from the initial domain as the plane wave tends to spread out. This decay in breather energy is accompanied by a slight increase in breather frequency until the frequency reaches $\Omega' = 1.0512$. Then the

breather no longer evolves. This behavior is easy to understand because the initial condition was such that $2\ \Omega$ was *inside the optical phonon band.* Due to the nonlinearity of the Morse potential the oscillation at frequency Ω also generated a $2\ \Omega$ contribution, which was responsible for the plane wave superimposed on the breather. In a finite lattice with periodic boundary conditions, this situation is compatible with a finite energy excitation which could be stable, as shown by the Floquet analysis. But in an infinite lattice, as the optical phonons are nonlocalized excitations, the solution can no longer be stable, unless it includes a phonon which is infinitely extended and therefore has an infinite energy. This is why the initial condition localized in the region of size N_0 decays. As the energy and frequency of a breather are linked, the decay causes a frequency shift until $2\ \Omega$ is above the optical band. This particular example indicates that the second condition of existence $m\Omega \neq \sqrt{\mathcal{V}''(0)}$, obtained in the anticontinuum limit, has to be extended to a nonresonance condition with the full optical band and not simply the bottom of the band. Frequencies Ω such that $2 \lesssim m\Omega < \omega_M$, where ω_M is the maximum of the optical band defined by Eq. (7), cannot correspond to stable breathers. These unstable frequency bands are indicated by the full lines in Fig. 4(a). At low K_+ the bands corresponding to different values of i are separated, but, as the optical band broadens for higher coupling, the various instability band overlap and the whole frequency range $\Omega < \omega_M/2$ leads to instabilities due to resonance with the optical band.

While the instability bands shown in Fig. 4(a) define sufficient conditions for a breather to be unstable, a frequency Ω outside of one of these bands does not guarantee stability. While the solution of Fig. 3(b) with $\Omega = 1.06$, i.e., such that $2\Omega > \omega_M = 2.0976$ for $K = K' = 0.1$ has no superimposed phonon as expected and does correspond to a stable solution, there are unstable solutions which are not determined by the forbidden frequencies shown in Fig. 4(a). This is particularly true at high coupling where the breathers are generally found to be less stable or at low frequency for small K_+ because the amplitude of the breather becomes then very large. Figure 5 shows the maximum amplitudes ($U - V$) and energies of the breathers versus their frequencies for a small coupling case $K = K' = 0.1$. The stable breathers (marked by diamonds) are found in the higher frequency range (except for the case $\Omega = 1.04$ discussed above which resonates with the optical band), but no stable breathers were found for $\Omega < 0.805$, although, according to the forbidden regions defined above, one could expect stability for $\omega_M/3 = 0.6992 < \Omega < 1$. Figure 5 shows that amplitude and energy rise sharply when Ω decreases below 0.8. This rise is well described by an approximate solution obtained by assuming that only the central site n_0 is moving while sites $n_0 \pm 1$ are at rest. Such a situation corresponds to an extremely narrow breather and the motion is simply the motion of a particle subjected to the combined action of the on-site Morse potential and the two harmonics springs of constant K connected to the fixed neighbors. The amplitude and energy of such a motion can be calculated exactly versus frequency, and, as shown in Fig. 5, this simplified picture gives a rather accurate description of the exact breather solution, and, in particular, explains the sharp rise in energy and amplitude found at low frequency.
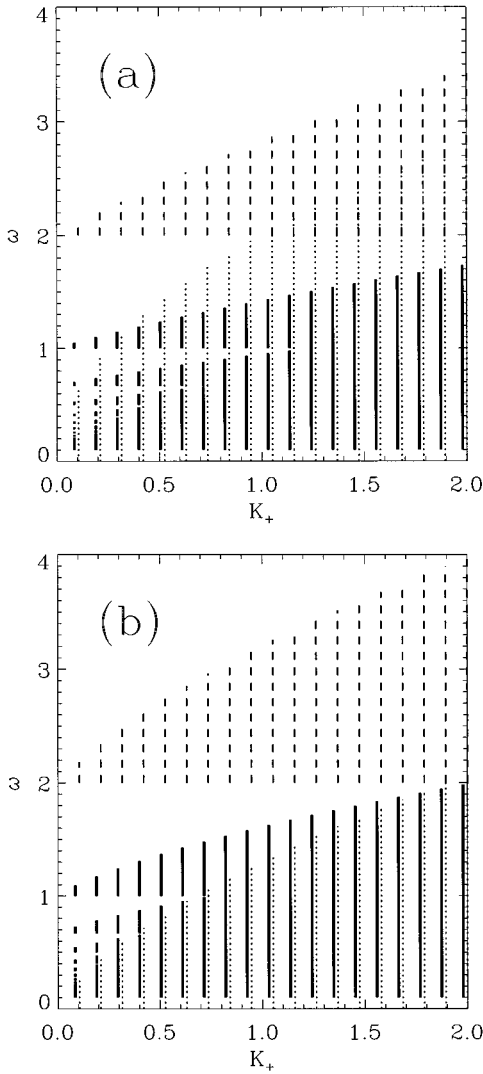
FIG. 4. Domains of instability for the breather frequency as a function of the coupling constant K_+ (a) for $K_- = 0$ and (b) for $K_- = 0.9 K_+$. For each value of K_+, the dashed line indicates the optical phonon band, the dotted line indicates the acoustic band, and the thick full lines correspond to the frequency domains, such that $i\Omega$ is within the optical band, for i integer ($2 \leqslant i \leqslant 20$).

Although the instability bands shown in Fig. 4 do not provide a complete view of the regions of existence and stability of breathers in a one-component model, they give, however, a rather precise picture of the domain where we can expect breathers in a one-component model. Let us now examine to what extent the same ideas can be applied to a two-component system.

2. $K \neq K'$, two-component system

In a two-component system the acoustic degree of freedom X is coupled to the optical variable Y. This shows up in the shape of the breather as illustrated in Fig. 6. Due to the different coupling constants along the two chains the amplitudes of the U and V displacements are different and $X = (U+V)/\sqrt{2}$ no longer vanishes. As mentioned in Sec. III A, this does not prevent the system from having exact localized breathers which are now two-component breathers. Figure 6 shows one example of such a solution, which is
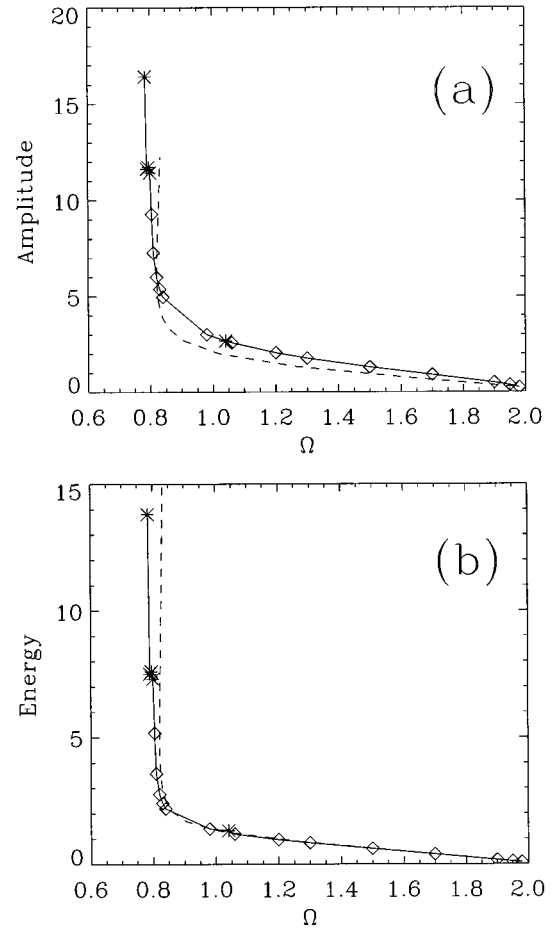

FIG. 5. Amplitudes (a) and energies (b) of the breathers for $K = K' = 0.1$ The diamonds and stars correspond to exact solutions which are, respectively, stable or unstable. The full line joins the points corresponding to exact solutions. The dashed line corresponds to the approximate results derived by assuming that only one particle is moving, its two neighbors being fixed at their equilibrium positions.

linearly stable and stable in a simulation in an ''infinite'' lattice. However, the domain of existence and stability of the two-component breathers is indeed affected by the presence of the second component. From the results obtained for a one-component breather, we can expect that resonances with the phonon bands may be a major cause of instability. Resonances of $m\Omega$ with the optical band are still possible and result in a first set of forbidden frequency bands. For $K \neq K'$ the optical band becomes slightly broader, as shown in Fig. 4(b) drawn for $K_- = 0.9 \, K_+$, i.e., a case where the two sublattices are very different ($K' = 0.053 K$). Consequently resonances with the optical band forbid larger domains in the breather frequencies. But the most important new feature is a possible resonance of the breather frequency with the acoustic phonon band. Instead of a higher order coupling ($m = 2, 3, \ldots$) as for the resonance with the optical band, it can be a first order coupling because Ω is situated below the optical band, i.e., in a possible frequency range for the acoustic modes. Figure 4 shows that, for small K_- the gap between the acoustic and optical modes disappears completely around $K_+ = 1.0$. Therefore we do not expect stable two-component breathers for $K_+ \geqslant 1$. However, for lower values
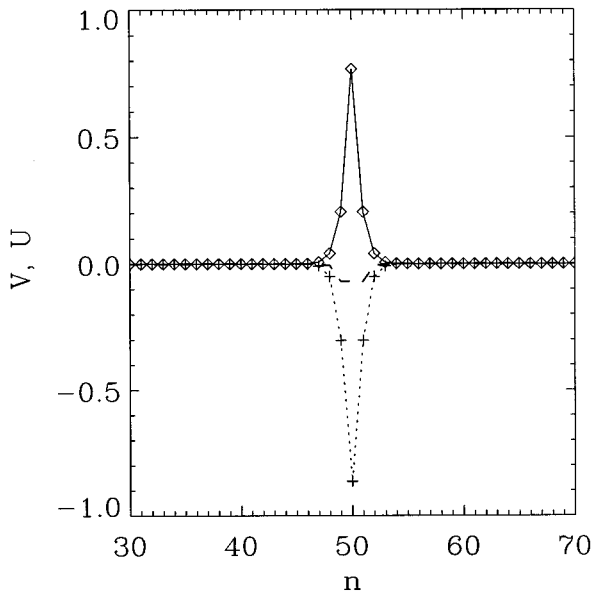
FIG. 6. Breather shape for $K=0.40$, $K'=0.12$, and $\Omega=1.6$. The diamonds and crosses show the initial positions of U_n and V_n, respectively, and the dashed line shows X_n.

of K_+, two-component stable breathers can exist provided that their frequency Ω lies in the gap between the acoustic and the optical modes. Moreover, such breathers are sufficiently stable to play the role of attractors for the solution if we start from a case where Ω is in the acoustic band. As described above for a case of a resonance with the optical band, a breather coupled to the acoustic band may loose enough energy for his frequency to move up above the acoustic band and reach a domain where the breather is stable. And even when there is no gap between the acoustic and optical bands, i.e., when we do not expect any stable breather, very long lived localized breathing modes may exist. This is illustrated in Fig. 7 for $K=1.7$, $K'=0.9$, and $\Omega=1.9$. Although $K_-=0.4$ implies a strong coupling with the acoustic modes as Ω is within the acoustic band, a simulation over more than 6000 breather periods shows only a small decay of the breather. There is indeed a constant energy loss through acoustic modes as shown in Figs. 7(a) and 7(c), but the breather is, nevertheless, extremely long lived.

Therefore, the numerical results for $K \neq K'$ show that, although the coupling between two degrees of freedom provides additional channels for energy loss away from a localized mode, stable two-component breathers do exist. For a small coupling constant K_+ their domain of stability is not very different in a one-component or in a two-component system, as shown by Figs. 4(a) and 4(b). For a large K_- the limiting factor for the stability is not the coupling with the acoustic modes but nonlinear resonances with the optical bands as for the one-component model. It is also important to notice for physical applications that the instabilities exhibited by the numerical studies are weak, for both the one-component or the two-component breathers. An ''unstable'' breather can oscillate for hundreds or even thousands of periods before decaying significantly, so that even breathers detected as unstable in this study can play a role in a physical system.
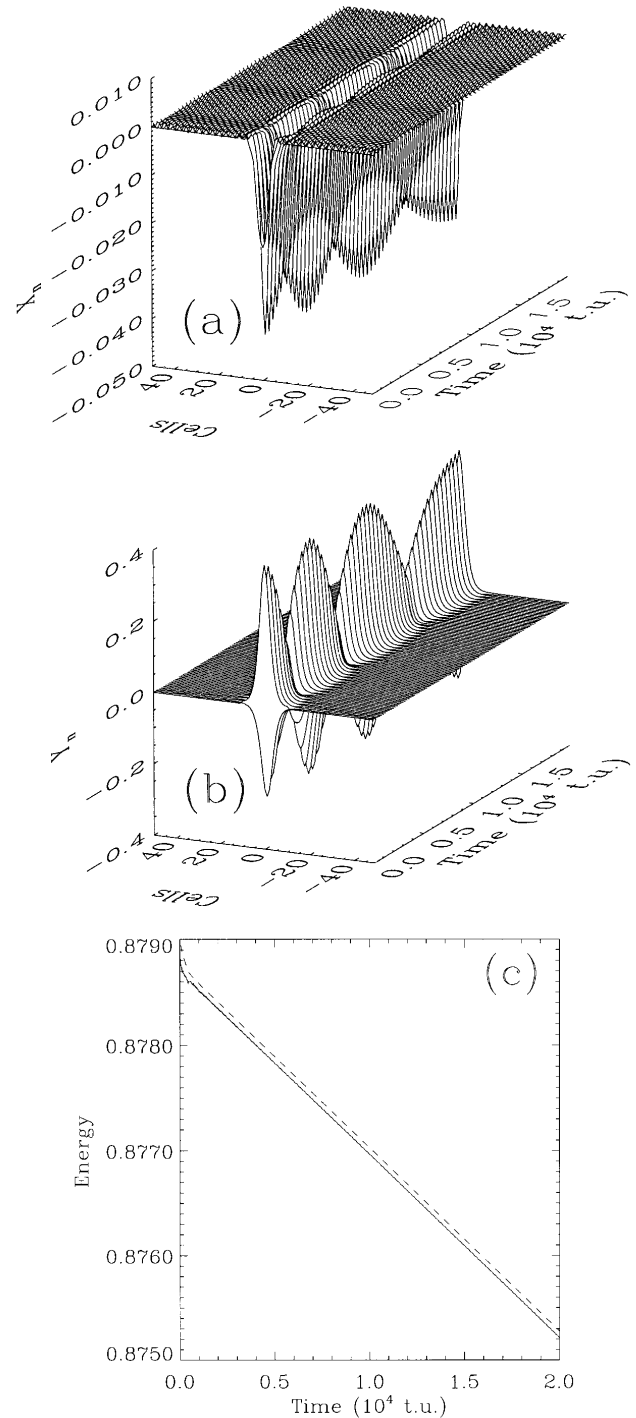

FIG. 7. Time evolution of a two-component breather in a system without gap between the acoustic and optical phonon bands. $K=1.7$, $K'=1.1$, $\Omega=1.9$. (a) X component at different times from 0 to 20 000 time units. The vertical scale extends from -0.05 to $+0.01$. (b) Y component. The vertical scale extends from -0.4 to $+0.4$. The apparent oscillation of the amplitude is due to a beating between the breather period and the recording period. This beating becomes slower as the time increases because the breather radiates acoustic waves which can be seen in (a). This energy loss is associated with a slow drift of the breather frequency to higher values. The beating provides a sensitive way to detect this frequency shift. (c) shows the breather energy (full line) and the total energy of the chain vs time. The decay is due to the acoustic waves emitted by the breather and absorbed by the damped boundary regions.
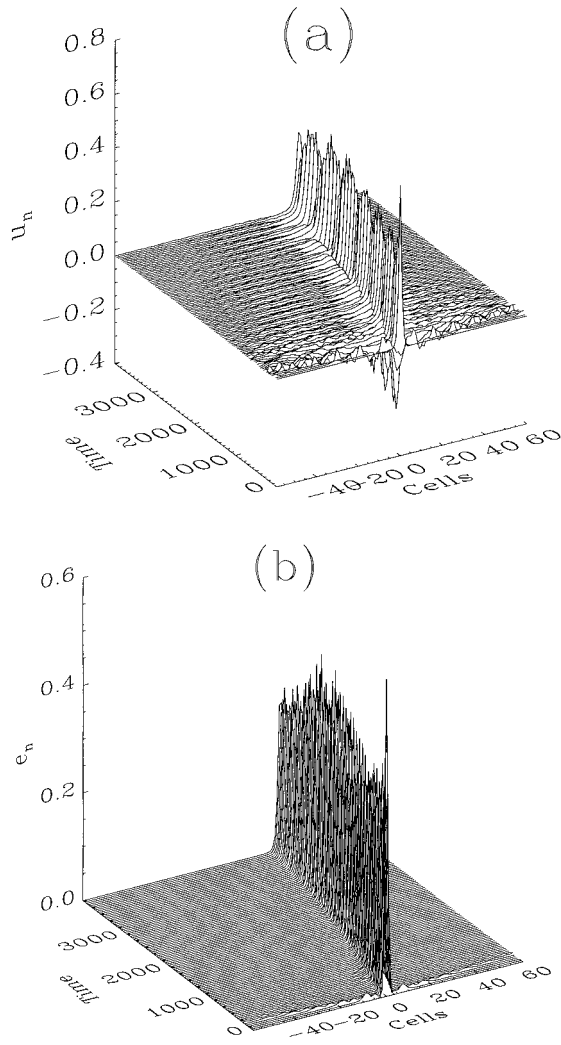
FIG. 8. Moving breather generated by the approximate solution (26) with $K=0.7$, $K'=0.5$, $q_1=0.1$, $V_e=0.01$. (a) Amplitudes U_n vs time. (b) Energy density e_n vs time. The oscillations of the amplitudes of the maxima are due to sampling effects; however, the maximum energy density shows a slow decay.

Up to now we have considered only exact initial conditions obtained by starting from the anticontinuum limit. It is useful to examine also the validity of the approximate solutions derived in Sec. III B, in particular, because Eqs. (26) and (27a) can correspond to breathers which are moving with respect to the lattice. Figure 8 shows one example of such a solution. The initial condition shows a fast evolution characterized by a decay of its amplitude and energy density by about 15% and an emission of small amplitude radiations. Simultaneously the frequency increases from $\Omega=1.64$ to $\Omega=1.83$. Then the solution is fairly stable. However, the velocity shows a slow decay and there is a weak energy loss that persists. This is because moving breathers are not exact solutions of the discrete lattice. We have discussed, for the one-component case, the difference in energy between the centered and noncentered breathers. The same is true for a two-component breather. Discreteness effects are responsible for the continuous energy loss that will eventually lead to a pinning of the breather at some site in the lattice. However, for the rather strong coupling $K_+=0.6$, large amplitude
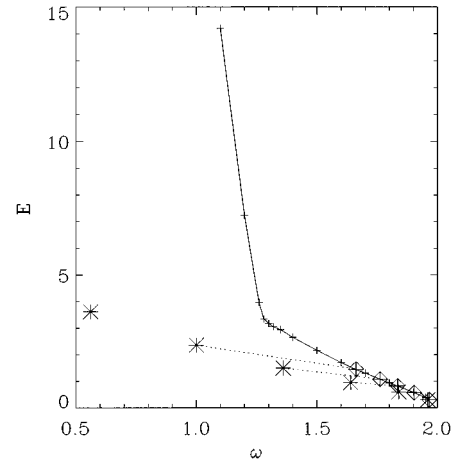

FIG. 9. Evolution of the approximate solutions of Eq. (26) when they are used as initial conditions in simulations in a system with $K=0.7$, $K'=0.5$. The stars show the energy vs frequency for each initial condition. The diamonds (connected to the corresponding initial point by a dotted line) show the energy vs frequency for the steady state solutions reached after 10 000 time units. (The initial condition around $\omega=0.5$ does not converge toward a localized breather.) The crosses connected by the full line show the exact breather solutions obtained numerically from the anticontinuum limit.

breathers can move long distances, as shown in Fig. 8. As for the one-component breathers [9], the pinning of two-component breathers increases with their amplitude. For instance, with $K=0.15$ and $K'=0.05$ a breather generated with the approximate initial condition with $q_1=0.1$ and an amplitude $a_0=0.3$ is immediately pinned while a breather generated with $a_0=0.05$ moves at the prescribed velocity $V_e=0.01$.

Figure 9 compares the energy-frequency dependence of the exact solution with that of the approximate solution (26), as it is initially and after the approximate initial condition has settled to a quasistable breather in a simulation. Although the initial breather parameters given by the approximate solution may be significantly different from the parameters of the exact solution, particularly for the frequency, Fig. 9 shows that, in a broad range of parameters, the approximate solution gives an initial condition that evolves toward an exact solution of the two-component model. Only the initial condition with $\Omega=0.56$ obtained with $a_0=0.6$ which corresponds to a narrow large-amplitude breather, which is certainly not properly described by the approximations leading to Eq. (26) failed to converge to a stable breather. This is another indication of the good stability of the two-component breathers since they can be generated from a initial condition which is far from exact.

The broad breathers obtained from the NLS equation are mobile in the lattice because their width is much larger than the lattice spacing and discreteness effects are averaged out on the spatial scale of the breather. There are other situations in which discreteness effects can become weak, even for narrow breathers. As mentioned above for the one-component model $K=K'$, a breather centered on a lattice site does not always correspond to the stable solution, which may be associated with the noncentered, or multibreather

[16], solution. Scanning through the breather frequencies one can check that there may be several values which correspond to an exchange of stability between centered and noncentered breathers. This feature, first noticed for the ϕ^4 model [14], has been studied in detail for the one-component model [17,18]. When an exchange of stability occurs, these studies show that even very narrow breathers can become very mobile in the lattice. The same exchange of stability between centered and noncentered breathers is found for the two-component model as for the one-component case.

IV. INTERACTIONS BETWEEN LOCAL MODES AND LOCALIZATION OF THERMAL FLUCTUATIONS

As the preceding section shows that two-component breathers are sufficiently stable to play a role in a physical system, it is important to study how they could be generated in a real system. We examine here a mechanism which has been shown to lead to large amplitude breathers in one-component systems, the collision between breathers with different amplitudes in a discrete lattice [4], and then we investigate the spontaneous localization of thermal fluctuations.

A. Collisions between breathers

The investigations have been carried out along the same lines as in the study of the one-component system. We are interested in the energy exchange between the colliding breathers. The studies of the one-component model have shown that the exchange is larger when the two colliding breathers have significantly different amplitudes. This is understandable because for two identical breathers, owing to the symmetry of the roles played by the two excitations, the energy exchange has to vanish. We consider here collisions between a large amplitude breather, henceforth called the big breather, which is initially fixed with respect to the lattice, and a mobile small-amplitude breather launched with an initial velocity toward the big breather. The big breather is an exact solution so that its energy is well defined and can be measured accurately. The small breather is an approximate solution given by Eqs. (26). As breathers are excitations with an internal degree of freedom, the outcome of their interaction depends on their relative phases at collision time. Consequently to analyze the mechanism that could lead to the formation of large breathers in a real system, we must scan all the relative phases of the two excitations. This is achieved by statistical sampling. We simulate 200 collisions with the same big breather and various small breathers with initial positions and initial velocities chosen at random with a Gaussian distribution around selected mean values. The width of the distribution is chosen large enough to cover all relative phases during the interaction and scan a rather broad range of amplitude and velocities of the small breathers.

To examine the collision quantitatively, we define the energy of the big breather $E_1(t)$ as the sum of the energy density on the 11 sites centered around its central site $n_1(t)$

$$E_1(t) = \sum_{n_1(t)-5}^{n_1(t)+5} \mathcal{H}_n(t), \qquad (28)$$

where $\mathcal{H}_n(t)$ is the energy density at site n extracted from the Hamiltonian (2). As the big breather is highly localized, the value of 11 sites is large enough to capture almost all its energy, and small enough to separate its energy from that of the small breather, except during a small time interval around the collision. We then define the transfer of energy from the small breather to the big one, $\Delta E_1(t)$, and the displacement of the large breather $\Delta n_1(t)$ as

$$\Delta E_1(t) = \frac{E_1(t) - E_1(0)}{E_2(0)}, \qquad \Delta n_1(t) = n_1(t) - n_1(0) \tag{29}$$

where $E_1(0)$ is the initial energy of the big breather and $E_2(0)$ is the initial energy of the small breather. With this definition $\Delta E_1 = 1$ if the big breather absorbs all the energy of the small one and $\Delta E_1 = 0$ if no energy has been transferred. In order to also investigate how the energy transfer is split between the optical and acoustic motions, we compute the quantities

$$\Delta E_1^x(t) = \frac{E_1^x(t) - E_1^x(0)}{E_2(0)}, \qquad \Delta E_1^y(t) = \frac{E_1^y(t) - E_1^y(0)}{E_2(0)} \tag{30}$$

where the quantities E_1^x, E_1^y denote the optical and acoustic contributions to the energy of the big breather calculated from the expression of the Hamiltonian as a function of the X and Y variables. Notice that $\Delta E_1^x(t)$ and $\Delta E_1^y(t)$ are always normalized by the total energy of the small breather. The quantities $\Delta E_1(t)$, $\Delta E_1^x(t)$, $\Delta E_1^y(t)$ show a fast variation during the collision process and then stay almost constant, although the big breather, perturbed by the collision, is no longer an exact solution and may radiate a small amount of energy for some time after the collision. Therefore it makes sense to speak of the values of these quantities ''after'' the collision without specifying their full time dependence. This is generally not true for $\Delta n_1(t)$ because, except for the most discrete case, the big breather is often set into motion by the collision. In this case Δn_1 is simply calculated from the final position $n_1(t)$ at the end of a simulation and its large value attests that the breather has gained a nonzero velocity in the collision.

Figure 10 compares typical results of two sets of 200 collisions for the symmetric case $K = K' = 0.6$ and the two-component model $K = 0.7$, $K' = 0.5$. The big breather is the exact solution with frequency $\omega_b = 1.70$, initially centered at site 100 of a 200 cell lattice and the small breather calculated with $q_1 = 0.1$ has an average amplitude parameter $a_0 = 0.15$ (variance 0.05), an average velocity $V_e + V_{g1} = 0.2$ (variance 0.1), and an average initial position 70 (variance 10). The figure shows histograms of the probability distribution of the energy transfers ΔE_1, ΔE_1^y, ΔE_1^x and displacements of the big breather Δn_1. The results of the two-component model are very similar to the results obtained earlier on the one-component model [4]. They show *that the mechanism of energy localization through breather collisions appears to be general and not restricted to a very simple one-component nonlinear lattice.* Although Fig. 10 shows that the energy transfer in favor of the big breather is slightly larger for the symmetric case $K = K' = 0.6$ than for the two-component model $K = 0.7$ $K' = 0.5$, for both models, the distribution of
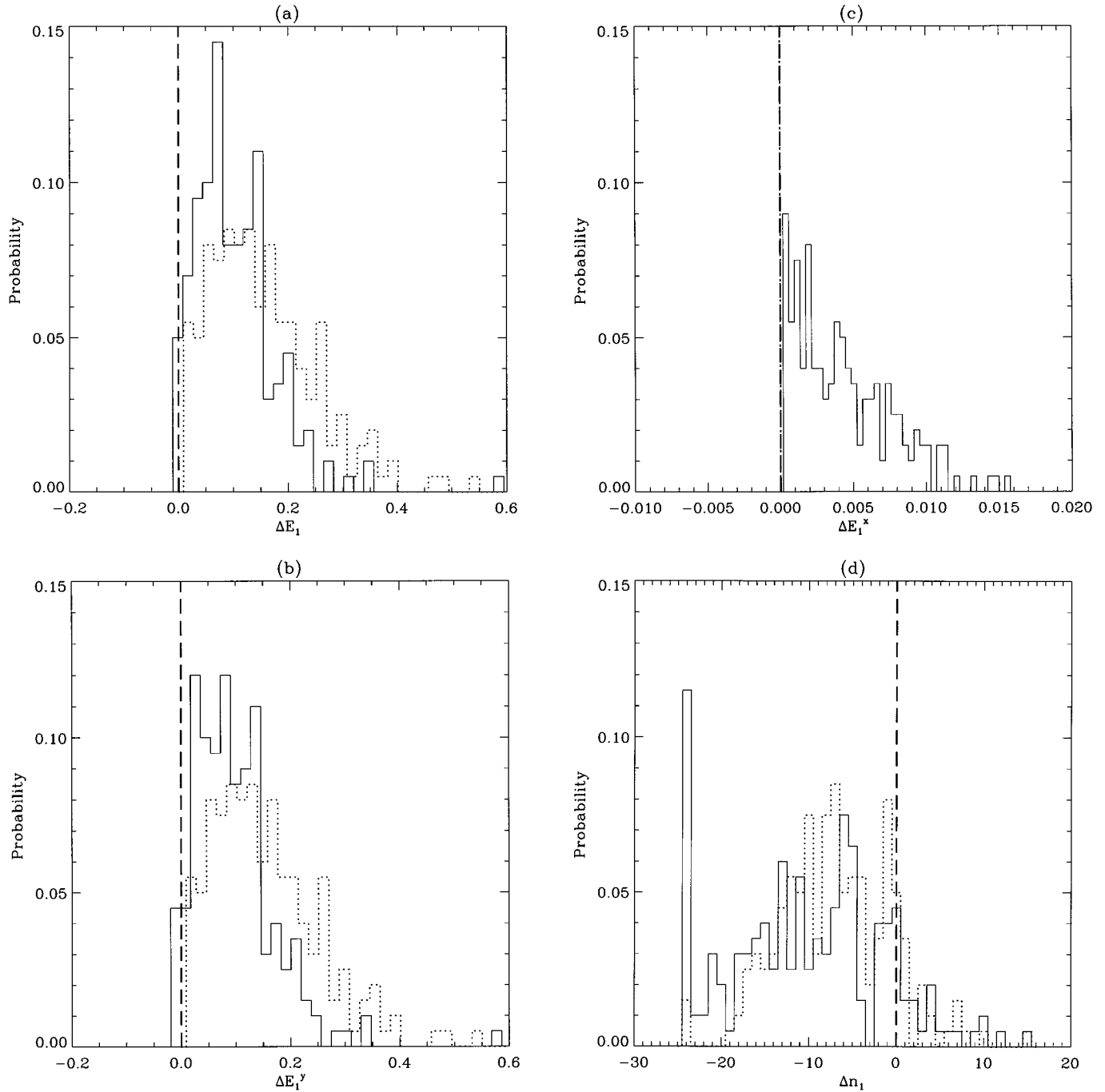
FIG. 10. Energy exchange in sets of 200 breather collisions for $K_+ = 0.6$. The dashed lines show the results for $K = K' = 0.6$ and the full lines show the results for the asymmetric case $K = 0.7$, $K' = 0.5$. (a) Histogram of the total energy exchange ΔE_1 showing the probability of a given value of ΔE_1 vs ΔE_1. Each histogram is generated by dividing the full range of ΔE_1 observed in the 200 collisions into 40 intervals and counting the collisions falling in each interval. (b) Histogram of the energy transfer to the optical motion ΔE_1^y. (c) Histogram of the energy transfer to the acoustic motion ΔE_1^x. For the symmetric case $K = K' = 0.6$ the acoustic motion is completely decoupled from the optical one and thus ΔE_1^x is always equal to 0. (d) Histogram of the displacement of the big breather Δn_1. The large peak at $\Delta n_1 = -25$ corresponds to the big breathers put into motion after the collisions, which have reached the limit of the investigated domain at the end of the simulation.

energy transfer is clearly biased toward positive values (only very few cases in the 200 collisions result in an energy loss for the big breather). Therefore random collisions between a small and a large breather tend to increase the energy of the larger breather. One should notice however that the collisions do not result in a complete absorption of the small breather by the big one. Although ΔE_1 reached 0.8 in some

rare events, on average only 10% to 15% of the energy of the small breather is lost in favor of the big one and the small breather passes through the big one (or, in some rare cases is reflected). The results shown in Fig. 10 do not correspond to a particular case. In all cases that we have investigated where we started from a *stable* big breather, we obtained similar results. The energy transfer in favor of the big breather is

larger when the discreteness effects are larger, but it is still observed for $K_+ = 1.0$ ($K = K' = 1.0$ or $K = 1.1$, $K' = 0.9$) or for higher big breather frequencies such as $\omega_b = 1.8$ for $K = K' = 0.6$ or $K = 0.7$, $K' = 0.5$. The distribution of the energy between the optical and acoustic motions shows that most of the transfer concerns the optical motion. Figure 10(c) shows that ΔE_1^x does not exceed 0.02, while ΔE_1^y reaches 0.6 in several cases (isolated cases up to 0.8 have been observed). If we start from an *unstable* big breather, which has a slow decay when it is left unperturbed such as the noncentered breather for $K = 0.7$, $K' = 0.3$, $\omega_b = 1.5$, the average value of ΔE_1 is negative. This is not surprising and it simply indicates that the collisions that perturb the unstable breather accelerate its decay. This may also give a clue to the origin of the energy transfer in favor of big breathers because it suggests that it is the most stable excitation which tends to gain energy. We do not have exact analytical solutions for the discrete breathers. This precludes any analytical estimate of the energy transfer which would require an accurate description of the collision since it is a small effect. However, the proof of existence of the discrete breathers [2,3], which indicates that there is a minimum value of the amplitude below which exact localized solutions no longer exist, supports the idea that big breathers are more likely to exist as localized excitations and therefore more likely to gain energy in collisions with small amplitude breathers which are only approximate solutions.

Figure 10(d) shows that the displacement of the big breather is often large and negative, i.e., in the direction of the incoming breather. The large peak at $\Delta n_1 = -25$ arises from the big breathers that were put in motion with a negative velocity after the collision. The high mobility of the big breather is due to the rather high coupling $K_+ = 0.6$ for this set of simulations and it is enhanced after the collision because small amplitudes which are radiated in the nonelastic collisions tend to induce a diffusion of the breather.

In the previous studies, a big breather is hit once by a small breather. The observed transfers of energy suggest that it is possible to raise progressively the energy of the big breather by multiple collisions. Figure 11 shows that this is indeed true, but the energy of the big breather is limited by the limit stability determined in Sec. III C. The initial collisions cause a large energy increase and the energy gain decays to zero when we reach a high energy, corresponding to low frequency, for which the isolated breather was found to be unstable. This result is consistent with the energy decay described above for the collisions with an unstable big breather. Although breather collisions can lead to energy localization in the nonlinear lattice, they cannot drive a breather into an energy-frequency range where it would be unstable, which puts an upper bound on the maximum energy of a localized excitation in the lattice. Multiple collisions cannot only boost the energy of a large stable breather, they can also prevent a weakly unstable breather from decaying, as illustrated in Fig. 12.

B. Spontaneous localization of thermal fluctuations

Breather collisions provide a mechanism for energy localization in a nonlinear lattice, but the studies described above to illustrate this mechanism consider a specially prepared
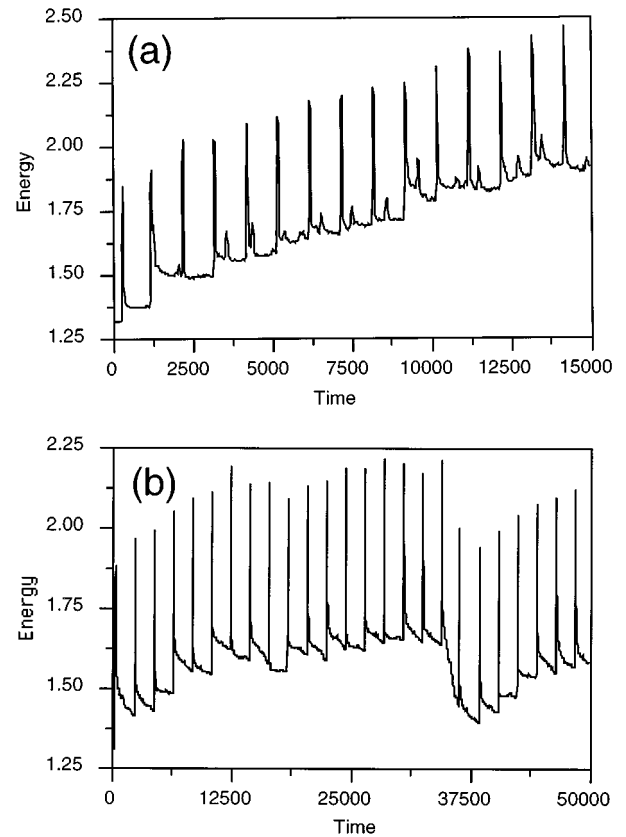

FIG. 11. Time evolution of the energy of a big breather undergoing multiple collisions with small breathers. The energy is measured in an 11 cell window around the center of the big breather. Each peak corresponds to a collision, when the small breather is inside the measurement window. (a) $K = K' = 0.6$, $\omega_b = 1.7$ and (b) $K = 0.7$, $K' = 0.5$, $\omega_b = 1.7$. Note that the time scale is not the same in the two figures. In case (b) we show a larger number of collisions. When the breather is driven up to an energy for which it is not stable it can show a sharp decrease and then grow again under the effect of subsequent collisions.

initial condition. If energy localization is to be important in a physical system, it has to occur naturally from the energy which can be brought to the system, i.e., from thermal energy. We know that this is possible in a one-component model [5]. The question that we want to address in this section is: is it still true in a multicomponent model where energy could be spread out by the acoustic modes? In order to answer this question, we have simulated the dynamics of the lattice in contact with a thermal bath at constrained temperature. This is achieved with an extended version of the Nosé-Hoover method [19], which completes the system by adding a small number of extra degrees of freedom, called "thermostats" which are coupled in a nonlocal way to all the physical degrees of freedom of the lattice. It can be shown that a microcanonical simulation of the extended system results in canonical equilibrium properties of the physical system of interest. We use a chain of three thermostats which provides good ergodic properties and we have checked that the first and second moments of the kinetic energy of the nonlinear lattice have their values expected in the canonical ensemble.

The numerical simulations confirm the results of the previous sections which indicate that the multicomponent model
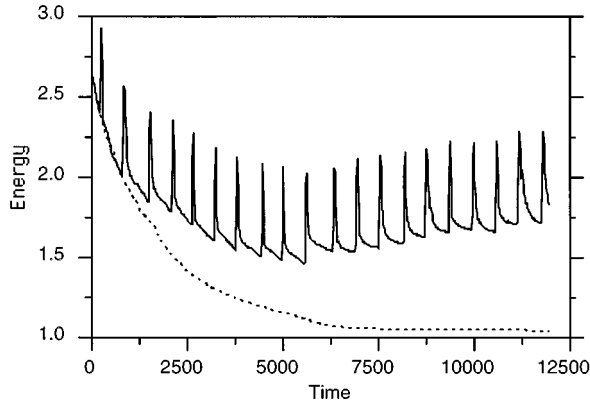
FIG. 12. Time evolution of the energy of a weakly unstable big breather undergoing multiple collisions with small breathers. $K=0.7$, $K'=0.5$. The big breather has frequency $\omega_b=1.4$ and the small breathers have an amplitude parameter $a_0=0.15$ and a velocity 0.15. The full line shows the energy of the big breather undergoing multiple collisions with incoming small breathers. The dotted line shows the time evolution of the energy of the same big breather without the collisions. It slowly decays until it reaches a stable state with a lower energy.

exhibits most of the properties of the one-component nonlinear lattice. Spontaneous localization of energy does occur in the multicomponent nonlinear lattice as illustrated in Fig. 13, which compares the case of the nonlinear lattice, described above to a harmonic lattice obtained by replacing in Hamiltonian (2) the on-site Morse potential by the harmonic potential $(U_n-V_N)^2$ which yields the same linear dispersion curves. Figure 13 has been obtained for a moderately discrete case $K_+=0.2$, and a large asymmetry between the two chains $K=0.3$, $K'=0.1$, i.e., $K_-=0.1$ in order to illustrate a case where the two types of displacements X and Y are strongly coupled. For other values of the parameters, the results are qualitatively similar but the tendency to localization decreases when K_+ increases, as one might expect from the previous sections, which have shown that the domain of existence of local modes is larger for a weak coupling.

Figure 13 shows that the harmonic and anharmonic lattice have very similar behavior for the acoustic motions. This was expected because, even for the Morse on-site potential, the equation of motion for X_n [Eq. (6a)] is linear. The only nonlinearity comes indirectly from the coupling with the Y_n displacements. It appears on a plot of the space-time Fourier transform $S_x(q,\omega)=\mathcal{F}(|X_n(t)|^2)$, which shows a broader dispersion curve for the anharmonic lattice than for the purely harmonic lattice. The X displacements appearing in Figs. 13(a) and 13(c) are dominated by the lowest frequency mode with wavelength $\lambda=2N$ in units of lattice cells because, for a given energy, it is the mode which has the largest amplitude. The calculation of $S_x(q,\omega)$ which shows a well defined maximum around the acoustic dispersion curve, indicates that an interpretation in terms of the linear phonon modes is meaningful for both the harmonic and the anharmonic lattices and that all modes are excited, as one can expect from a thermalized system.

On the contrary the optical motions are extremely different for the harmonic and anharmonic lattices. For the harmonic lattice, the results can be interpreted in terms of equipartition of energy among nonlocalized phonon modes. For
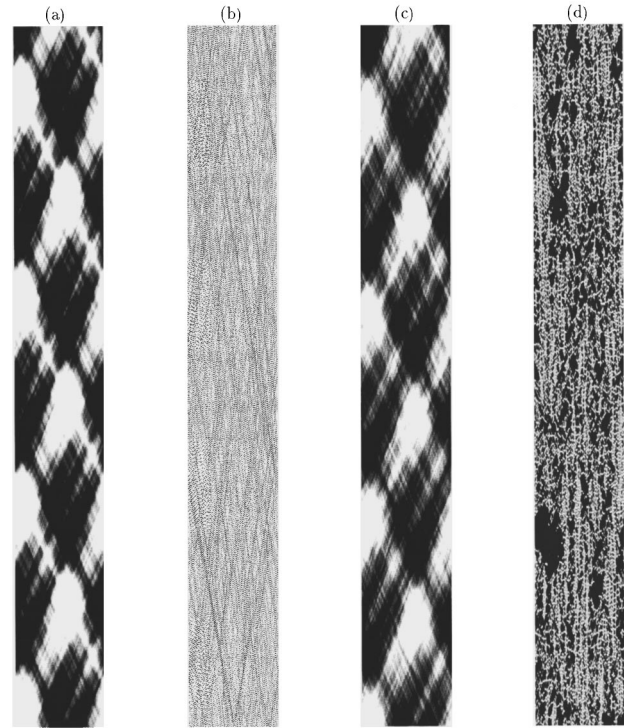

FIG. 13. Comparison of the properties of a linear (harmonic on-site potential) and nonlinear (Morse on-site potential) thermalized lattice. The coupling constants are $K=0.3$, $K'=0.1$ for both lattices. The temperature is $T=0.8$ in energy units. The gray scale figures show the X and Y displacements of the different lattice sites vs time. The horizontal axis extends along the lattice which has 128 cells with periodic boundary conditions. The vertical axis is the time axis. It extends over 1000 time units, i.e., 500 periods of the lowest optical mode. (a) Harmonic on-site potential: X_n (acoustic displacements). Gray scale from $X<-10$ (white) to $X>+10$ (black); (b) harmonic on-site potential: Y_n (optical displacements). Gray scale from $Y<-1$ (white) to $Y>+1$ (black); (c) Morse on-site potential: X_n (acoustic displacements). Gray scale from $X<-10$ (white) to $X>+10$ (black); (d) Morse on-site potential: Y_n (optical displacements). Gray scale from $Y<-0.5$ (white) to $Y>+5$ (black).

the rather weak coupling that we consider here $K_+=0.2$, the dispersion of the optical branch is small so that all modes have a similar amplitude. This results in the almost uniform gray tone of Fig. 13(b) that shows the $Y_n(t)$ displacements in the harmonic lattice. The calculation of $S_y(q,\omega)=\mathcal{F}(|Y_n(t)|^2)$ in this case reveals the expected dispersion curve of the optical phonon modes. For the anharmonic lattice, Fig. 13(d) shows that, on the contrary the notion of nonlocalized phonon modes completely loses its meaning. Moving along any horizontal line in Fig. 13(d), i.e., moving along the lattice for a given instant of time, one crosses regions with very large Y_n (up to $Y_n\approx15.0$) next to regions where Y_n is small ($-0.5<Y_n<0.5$). And it is remarkable that this pattern is almost conserved if one considers a time translation by moving the observed line up or down. In fact one can notice in Fig. 13(d) almost vertical lines where black and white spots alternate. They correspond to cells that oscillate between $Y<-0.5$ and $Y>5.0$ while nearby cells show only a very small amplitude motion. These lines are simply the local modes that we analyzed in the previous

FIG. 14. Optical displacements Y_n shown with a gray scale as in Fig. 13 in the anharmonic lattice for $T=0.3$. The lattice parameters are the same as for Fig. 13. Gray scale from $Y<0$ (white) to $Y>+1.5$ (black)

sections. They have been formed thermally and, at the high temperature $T=0.8$ (in energy units, to be compared to the dissociation energy equal to 1 for the Morse potential) that we have investigated to generate Fig. 13 some modes have a very high amplitude and low frequency. These local modes give rise to a very large central peak in $S_y(q,\omega)$ while the optical phonon branch is no longer visible. It is important to notice that, if one considers the behavior of the nonlinear lattice on a time scale of the order of $\Delta t=200$ [one-fifth of the time interval shown in Fig. 13(d)] *there is no equipartition of energy* among the various lattice sites. The sites with a large amplitude breather mode have a significantly higher energy density than others. While the largest breathers seen in Fig. 13(d) do not have a long lifetime, which is consistent with the fact that they have been found to be unstable in Sec. III, smaller breathers created thermally can persist for at least 50 to 100 oscillation periods. Equipartition of energy is only recovered if one averages over a much longer time scale (typically 500 to 1000 periods of the oscillations in the bottom of the Morse potential).

The simulation shown in Fig. 13 shows that thermal fluctuations can self-localize to form the breather modes investigated in the preceding section. This simulation has been performed for the high temperature $T=0.8$, but the formation of breathers is observed at much lower temperatures such as $T=0.3$, as shown in Fig. 14. However, at such low temperatures, the calculation of $S_y(q,\omega)$ shows a broad optical band in addition to the central peak, which indicates that extended modes coexist with the localized breathers although their frequency is below the frequency given by the linear dispersion curve.

V. ROLE OF BENDING ON DNA OPENING

The mechanism by which RNA polymerase opens locally the DNA double helix to initiate the transcription is not known, but there is experimental evidence that it involves a bending of the double helix [6,7]. Although it cannot claim to describe accurately the actual effect of the bending of a three-dimensional helix, the two-component model can bring insight into this mechanism. Using a simple mechanical model of the double helix, it is easy to observe the effects of a local bend: (i) Bases inside the bend are brought closer to each other while the ones which are outside increase their relative distance. This must modify the stacking interaction, increasing the coupling constant on the strand inside the bend while simultaneously decreasing the coupling constant along the outward strand. (ii) A local unwinding of the helix occurs in the middle of the bent region while the two regions next to the bend on both sides are on the contrary slightly more twisted. This is due to the rigidity of the two strands entangled in the double helix.

Molecular dynamics studies [20] show that DNA bending is accompanied by a significant reduction of the opening energy of the base pairs, which can be considered as the consequence at the microscopic level of the mechanical effects mentioned above. Contrary to the one-component model, the two-component model has enough freedom to describe both of these mechanical effects. The local variation of the stacking, which leads to different coupling constants on the two strands, simply corresponds to local changes in K and K'. The local bending corresponds to a local deviation of the acoustic degree of freedom X_n from its equilibrium zero value. This is not an equilibrium state of the free molecule, which would be straight, but it can be obtained by imposing on the X_n local constraints that correspond to the action of the bending protein. In the actual bending of DNA both mechanical effects occur simultaneously. However, for a better understanding of their influence on the localized modes, we have considered them separately.

In order to investigate the effect of a local variation of the stacking interaction, we have simulated cases where $K=K'$ almost everywhere, except in a central region of the chain, extending over 20 cells, where $K \neq K'$. The influence of such an extended defect on moving breathers depends heavily on the choice of parameters. It may cause breather reflection, temporary trapping, or on the contrary a speed-up when the breather passes through the perturbed region. Consequently, although one can find some parameter range in which the defect causes breather trapping and therefore promotes DNA opening, the rather weak effect of stacking alteration and its sensitivity to parameters suggest that it is not the main mode of action of RNA polymerase.

Numerical simulations of the direct effect of bending indicate that the geometrical deformation induced by the enzyme can play a more systematic role to favor opening than the change that it induces on the coupling constants. Structural studies of the DNA protein complex show that, in order to bend DNA, RNA polymerase makes contact with the helix in two regions [21,22]. This can be simulated by imposing constraints on the X_n in two regions around the center of the bend. We assumed a linear variation of the X_n in these constrained regions through the conditions

$$X(n_c - n_b + i) = i\alpha, \quad X(n_c + n_b - i) = i\alpha$$

$$\text{for} \quad 0 \leq i \leq n_W,$$

(31)

where n_c is the index of the central site of the bend, n_b gives the distance, in cells, from the center of the last bases constrained by the protein, and n_W is the width of the two contact regions [to improve the readability of the indices we have used the notation $X(n)$ instead of X_n]. The equilibrium configuration is obtained by minimizing the energy of the lattice with all other degrees of freedom allowed to evolve. Figure 15 shows an example of the shape of a relaxed lattice with $K = 0.2$, $K' = 0.8$, $n_b = 10$, and $n_W = 9$. The bend imposed on the acoustic coordinate X induces a local variation of the base pair stretching Y which is positive in the central part (corresponding to local unwinding) and negative on the two sides of the bend (corresponding to base in a pair squeezed together). This is consistent with the shape expected from the mechanical properties of a three-dimensional helix. One can notice that, if K and K' are exchanged, i.e., if we bend the lattice with the strongest strand inside the bend, in the planar two-chain model, the bend tends on the contrary to close the base pairs in the center.

The small value of Y in the vicinity of the bend shows that, in the two-chain model, the coupling between bending and opening, which is only due to the asymmetry $K \neq K'$ is weak compared to the coupling imposed by the three-dimensional structure of DNA. It has, nevertheless, a significant effect on the localized modes. We have studied it numerically with a method very similar to the one used to study breather collisions in Sec. IV. The big breather is simply replaced by the bend and small breathers with a Gaussian distribution of amplitude, and velocities are sent toward the bent region. The simulations are performed in terms of the variables X_n and Y_n, which allows us to maintain the bend by constraining the appropriate X_n coordinates as described above. The energy in the region $n_c - 2n_b \leq n \leq n_c + 2n_b$ is monitored versus time, as well as the energy density in the lattice.

As one might expect, the results depend on the characteristics of the bend, i.e., its spatial extension (determined by n_b and n_W) and its amplitude (determined by α). Broad bends are almost transparent to localized modes. On the contrary, sharp bends restricted to $n_W = 3$ or 4 cells can reflect most of the incoming local modes because their width is comparable to the width of the localized modes in a rather discrete lattice ($K_+ \leq 0.5$). This may have some consequences on the biological function because proteins often bend DNA sharply (90° bends resulting almost entirely in two 40° kinks extending only on a few base pairs have been observed [7]). Studies of the two-chain model suggest that such bends could be very efficient in preventing the transmission of localized excitations, and even linear phonon modes, across the bend region. Two such bends would almost isolate one region of the molecule from the remaining parts regarding the transmission of thermal fluctuations, and, for instance, energy delivered between the two bends by a chemical reaction would hardly flow away. Figure 16 shows the effect of a moderate bend ($n_b = 10$, $n_W = 9$, $\alpha = 0.12$, corresponding to the relaxed structure shown in Fig. 15). The
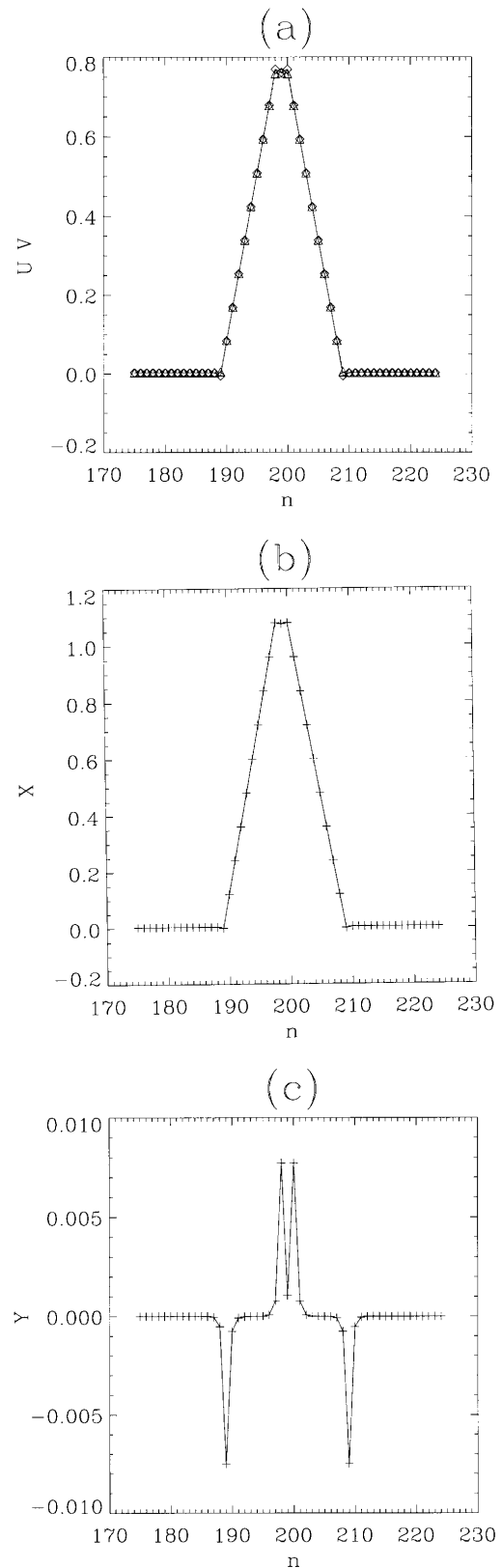

FIG. 15. Relaxed structure of the two-chain lattice in the presence of a bending constraint on X_n with $n_b = 10$, $n_W = 9$, $\alpha = 0.12$. The coupling constants are $K = 0.2$, $K' = 0.8$. (a) U_n and V_n coordinates of the particles, (b) X_n. The constrained sites correspond to the two inclined linear parts of the curve, (c) Y_n. The base-pair stretching induced by the bend is small and does not appear clearly in (a).
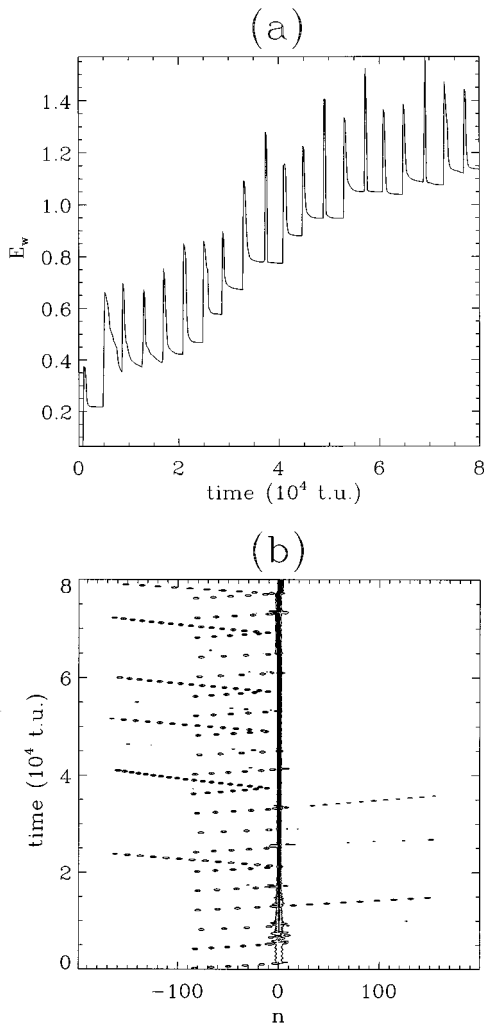
FIG. 16. Effect of a bend on incoming moving localized excitations in the two-chain model. The parameters of the model and the constraints imposed to create the bend are the same as for Fig. 15. (a) Energy density in a window of size $2n_b$ centered on the bend vs time (in dimensionless time units). Each spike corresponds to an incoming moving breather. (b) Contour plot of the energy density in the two-component chain vs time. The bend is centered on the site $n = 0$ and the breathers are launched every 4000 time units from site -100 with a positive velocity. They appear on the figure as lines of oval shaped patterns which are generated by the sampling of the breather energy density every 100 time units.

moving localized modes sent toward the bend had an amplitude $a_0 = 0.15$ (with a standard deviation $\sigma = 0.02$) and a velocity 0.1 ($\sigma = 0.01$). Figure 16(a), displaying the time evolution of the energy in the bent region, shows that the bend can act as an *energy collector*. While a few localized modes pass through or are almost totally reflected, as shown in Fig. 16(b), many of them are captured at the bend or at least abandon a large part of their energy in the bent region in the bent region. As a result the fluctuational opening of the base pairs increases drastically in the bent region. If the same mechanism could operate in the three-dimensional structure of DNA, it could explain how the RNA polymerase could create a transcription bubble without bringing in energy through chemical reactions.

VI. CONCLUSION

The model considered in this work was initially motivated by the study of DNA denaturation, but the most important results are probably the general conclusions that can be drawn for nonlinear energy localization in lattices. Studies of one-component lattices had previously shown that intrinsic local modes, due to nonlinearity, could exist in homogeneous lattices and that these modes could be spontaneously formed through localization of thermal fluctuations, one mechanism of their growth being energy exchanges in collisions that tend to favor the largest excitation. Consequently local modes could appear as involved in several physical phenomena, such as DNA denaturation, because they were likely to form in a nonlinear lattice as soon as the temperature was not too low.

However, in spite of these remarkable properties the relevance of local modes in a real system could be questioned because the vast majority of physical systems require a multicomponent description. Extra degrees of freedom provide additional channels for energy transfer so that it was not clear whether local modes could persist long enough in a realistic system to play a significant role. Using a two-chain model, we have shown that they do exist as exact solutions and that they have a broad range of stability. Moreover, we have shown that, even when we chose on purpose a case where a local mode should decay because its frequency resonates with a mode corresponding to another degree of freedom (a phonon mode of the acoustic branch), the decay is very slow. The lifetime of local modes is thus large enough to allow them to play a role in a physical process. Perhaps, more importantly for the physics, we have shown that the mechanism of growth of the local modes through energy exchange in collisions is still active, and that the spontaneous formation of local modes in a thermalized system takes place in the two-component model as it does in the one-component case. Of course, physical systems are often complex and a two-component order parameter may not be enough to describe them. Let us emphasize, however, that moving from one component to two components is a *qualitative jump* because we start providing external channels for the decay of local modes. Adding more than two components in a one-dimensional model may increase the decay rate of localized modes, but does not bring a qualitative change. It may happen that more components close completely the gap that separates the optical branch carrying the local modes from the other branches associated with the other degrees of freedom. But we have verified that, even when localized modes resonate with extended linear modes their lifetime may be very large.

One should, however, notice that the present results are restricted to a one-dimensional model. Investigations of multidimensional lattices [1] have already shown that they can sustain local modes. The question of their spontaneous formation is still open, and currently under study. We have considered here nonlinear lattices with an on-site potential. Local modes exist also in the presence of nonlinear coupling, without substrate potential, but their properties in multicomponent systems or in the presence of thermal fluctuations have yet to be studied.

Regarding the application to DNA, our results have to be

taken with caution because the two-chain model lacks a fundamental ingredient, the helicoidal structure of DNA. It is, however, important to notice that the local modes that we proposed earlier as possible candidates to describe the fluctuational openings observed experimentally still exist if we consider a more realistic DNA model than the one-component model examined earlier. It is also interesting to remark that, in spite of its simplicity, the two-chain model exhibits a coupling between bending and opening which seems to be an important feature in several biological functions. Although the extent of the coupling between these two degrees of freedom is much smaller in the two-chain model than in a three-dimensional helicoidal structure, it generates qualitatively the expected opening effect, and our results show that it can provide an energy collection mechanism for the transcription-enzyme activity, or that sharp bending could act as an ''insulator'' for the transmission of information by large amplitude fluctuations along the DNA molecule. These two aspects will deserve further investigations concerning their biological implications.

[1] S. Takeno, K. Kisoda, and A.J. Sievers, Progr. Theor. Phys. Suppl. **94**, 242 (1988); K. Hori and S. Takeno, J. Phys. Soc. Jpn. **61**, 2186 (1992).

[2] R.S. MacKay and S. Aubry, Nonlinearity **7**, 1623 (1994).

[3] S. Aubry, Physica D (to be published).

[4] T. Dauxois and M. Peyrard, Phys. Rev. Lett. **70**, 3935 (1993); O. Bang and M. Peyrard, Phys. Rev. E **53**, 4143 (1996).

[5] T. Dauxois and M. Peyrard, Phys. Rev. E **47**, 684 (1993).

[6] H. Heumann, M. Richetti, and W. Werel, EMBO J. **7**, 4379 (1988).

[7] S.C. Schultz, G.C. Shields, and T.A. Steitz, Science **253**, 1001 (1991).

[8] W. Saenger, *Principles of Nucleic Acid Structure* (Springer-Verlag, Berlin, 1984).

[9] O. Bang and M. Peyrard, Physica D **81**, 9 (1994).

[10] S. Aubry (unpublished).

[11] J.L. Mariñ and S. Aubry, Nonlinearity **9**, 1501 (1996).

[12] C. Eilbeck and J. Wattis, in *Nonlinear Excitations in Physics and Biology*, edited by M. Remoissenet and M. Peyrard (Springer-Verlag, Berlin, 1991).

[13] M.P. Calvo and J.M. Sanz-Serna, J. Sci. Comput. **14**, 1237 (1993).

[14] D.K. Campbell and M. Peyrard, in *Chaos/Xaos: A Soviet-American Perspective on Nonlinear Science*, edited by D.K. Campbell (AIP, New York, 1990).

[15] S. Flach and C.R. Willis, Phys. Rev. Lett. **72**, 1777 (1994).

[16] T. Cretegny and S. Aubry (unpublished).

[17] J.L. Mariñ, T. Cretegny, and S. Aubry (unpublished).

[18] Ding Chen, S. Aubry, and G. Tsironis, Phys. Rev. Lett. **77**, 4776 (1996).

[19] G.J. Martyna, M.L. Klein, and Mark Tuckerman, J. Chem. Phys. **97**, 2635 (1992).

[20] J. Ramstein and R. Lavery, Proc. Natl. Acad. Sci. USA **85**, 7231 (1988).

[21] A.Z. Ansarl, J.E. Bradner, and T.V. O'Halloran, Nature (London) **374**, 371 (1995).

[22] D. Erie, Y. Guoliang, H.C. Schultz, and C. Bustamante, Science **266**, 1562 (1994).